

Supplementary Information

Pushing the limit of layered transition metal oxide cathodes for high-energy density rechargeable Li ion batteries

U.-H. Kim,^{*a} D.-W. Jun,^{*a} K.-J. Park,^a Q. Zhang,^b P. Kaghazchi,^c D. Aurbach,^{*d} D. T. Major,^d G. Goobes,^d M. Dixit,^d N. Leifer,^d C. M. Wang,^e P. Yan,^e D. Ahn,^f K.-H. Kim,^g C. S. Yoon,^{*h} and Y.-K. Sun^{*a}

^a Department of Energy Engineering, Hanyang University, Seoul, 04763, South Korea. E-mail: yksun@hanyang.ac.kr

^b Physiklische und Theoretische Chemie, Freie Universität, Berlin, D-14195, Germany.

^c Forschungszentrum Jülich GmbH, Institute of Energy and Climate Research (IEK-1), Materials Synthesis and Processing, Wilhelm-Johnen-Straße, 52425 Jülich, Germany.

^d Department of Chemistry and BINA (BIU institute of nano-technology and advanced materials), Bar-Ilan University, Ramat-Gan, Israel 5290002. E-mail: aurbach@mail.biu.ac.il

^e Energy and Environmental Directorate, Pacific Northwest National Laboratory, 902 Battelle Boulevard, Richland, WA 99352, USA.

^f PLS-II Beamline Division, Pohang Accelerator Laboratory (PAL), Pohang, 37673, South Korea.

^g Global Frontier Center for Hybrid Interface Materials, Pusan National University, Busan 609-735, South Korea.

^h Department of Materials Science and Engineering, Hanyang University, Seoul, 04763, South Korea. E-mail: csyoon@hanyang.ac.kr

*Correspondence to: csyoon@hanyang.ac.kr, aurbach@mail.biu.ac.il and

yksun@hanyang.ac.kr

‡These authors contributed equally to this work.

Density-functional theory calculations

Density functional theory (DFT) calculations have been carried out using the projector-augmented plane-wave (PAW) method as implemented in the Vienna Ab Initio Simulation Package (VASP)^{1,2}. The exchange-correlation energy was described by the generalized-gradient approximation with the Hubbard U parameter (GGA+U)^{3,4}. U – J value for Ni was set to 1.0 eV. To make a direct comparison between total energies of bulk $R\bar{3}m$ and $Fm\bar{3}m$ we constructed a conventional unitcell with lattice parameters of $a=17.37 \text{ \AA}$, $b=11.53 \text{ \AA}$, $c=16.34 \text{ \AA}$, $\alpha=90^\circ$, $\beta=90^\circ$, $\gamma=90^\circ$ for $R\bar{3}m$ and $a=15.98 \text{ \AA}$, $b=8.22 \text{ \AA}$, $c=24.71 \text{ \AA}$, $\alpha=90^\circ$, $\beta=90^\circ$, $\gamma=90^\circ$ for $Fm\bar{3}m$ with the same number of atoms (96 Li, 96 Ni and 192 O). A k -point mesh of $1 \times 2 \times 1$ and energy cutoff of 450 eV were used for all bulk and surface structures. The convergence criteria for total energy were set at 10^{-4} eV. We used 8 and 12 layers slabs to model the surfaces of $R\bar{3}m$ and $Fm\bar{3}m$, respectively, and kept fixed 2 bottom layers for each structure. A vacuum space of 12 Å was introduced between slabs.

To find the structure of disordered bulk rock salt LiNiO_2 we have considered the following configurations: (i) six ordered (001) layers in a $2 \times 2 \times 3$ unit cell, (ii) six disordered (001) layers in a $2 \times 2 \times 3$ unit cell, (iii) two ordered and four disordered (001) layers in a $2 \times 2 \times 3$ unit cell, (iv) one ordered and five disordered (001) layers in a $4 \times 2 \times 3$ unit cell as well as (v)-(vi) two different six disordered (001) layers in a $4 \times 2 \times 3$ unit cell. Structures with some-ordered-(001) layers are more favorable than all-disordered-(100) layers ones for both considered unit cells. The structure (iii) is the most favorable one among all studied configurations. We used this structure in our study after enlarging its unit cell to $4 \times 2 \times 6$ which is needed to model a W dopant concentration of about 2%. For surface energy and O release energy calculations, we focused on structures with disordered subsurface layers but ordered termination for the following reasons. (i) The number of distinguishable O sites for an ordered termination is small. Since we have 392 atoms in our structure (2208 electrons) we cannot compute O release energy for many possible surface O vacancy sites. (ii) We are mainly interested in the effect of changes in crystal structure on the stability rather than local arrangement of surface cations. To calculate surface energies, we used the following equation

$$\gamma = \gamma_1 + \gamma_2 = \frac{E_{\text{surf}} - E_{\text{bulk}}}{2A}$$

where E_{surf} and E_{bulk} are the total energy of surface and bulk structure, respectively. A is the surface area of slab. The oxygen removal energy was calculated using

$$E_r = E_{\text{VO}} - E_{\text{pristine}} + 1/2E_{\text{O}_2}$$

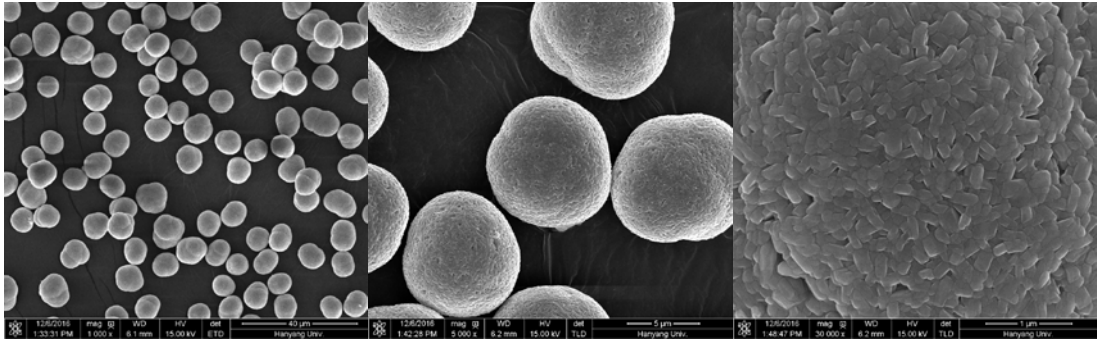
Here, E_{VO} , E_{pristine} , and E_{O_2} are total energy of the surface with O vacancy, the surface without vacancy, and an oxygen molecule in vacuum, respectively.

Charge compensation mechanism and super-exchange interactions.

To better understand the stabilizing effect of W-doping we analyzed the spin states of the ions in the systems modeled (Table S2). In $\text{Li}_{0.5}\text{NO}_2$, we have exclusively Ni^{3+} and Ni^{4+} ions, which formally have zero and one unpaired electrons in the d-orbitals. W-doping suppresses the presence of Ni^{3+} (Jahn-Teller active) and Ni^{4+} ions, while inducing formation of Ni^{2+} ions (formally two unpaired electrons), which is seen by the increased local magnetic moments on selected Ni atoms. This is due to charge compensation, i.e. the W^{6+} ion forces a lower charge of the Ni-ions, to keep balance in the system. In the rocksalt phase (i.e. $\text{Li}_{0.33}\text{Ni}_{0.67}\text{O}$ and $\text{Li}_{0.33}\text{Ni}_{0.625}\text{W}_{0.0417}\text{O}$), we observe almost exclusively Ni^{2+} ions, and we note that the average magnetic moment is considerably higher in the W-doped material (0.98 vs 1.17 μB , Table S2).

In several calculations, we observed spin-flipping during the calculations, which could be indicative of super-exchange interactions, as the spins arrange to minimize the total energy. This spin flipping of Ni^{2+} occurred during the self-consistent field electronic structure calculation (i.e. we started with initial ferromagnetic states), giving more stable models. This is more prevalent in the rocksalt phases that are rich in Ni^{2+} ions (Table S2), and this spin-flipping likely results in favorable super-exchange interactions with linear $\text{Ni}^{2+}(\text{down})\text{-O-Ni}^{3+}(\text{up})$ configurations.

a



b

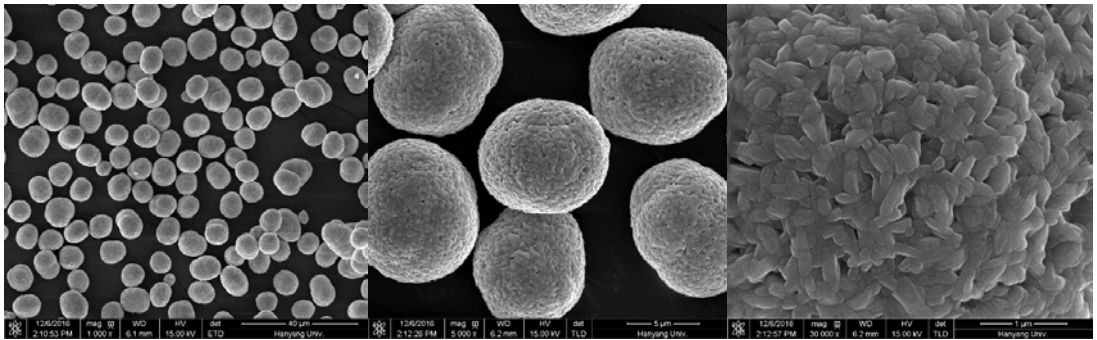


Fig. S1 SEM images of as-prepared LNO and 1 mol% W-LNO at different magnifications displaying uniform spherical morphology. Each particle was composed of nano-sized primary particles. (a) LNO. (b) 1 mol% W-LNO.

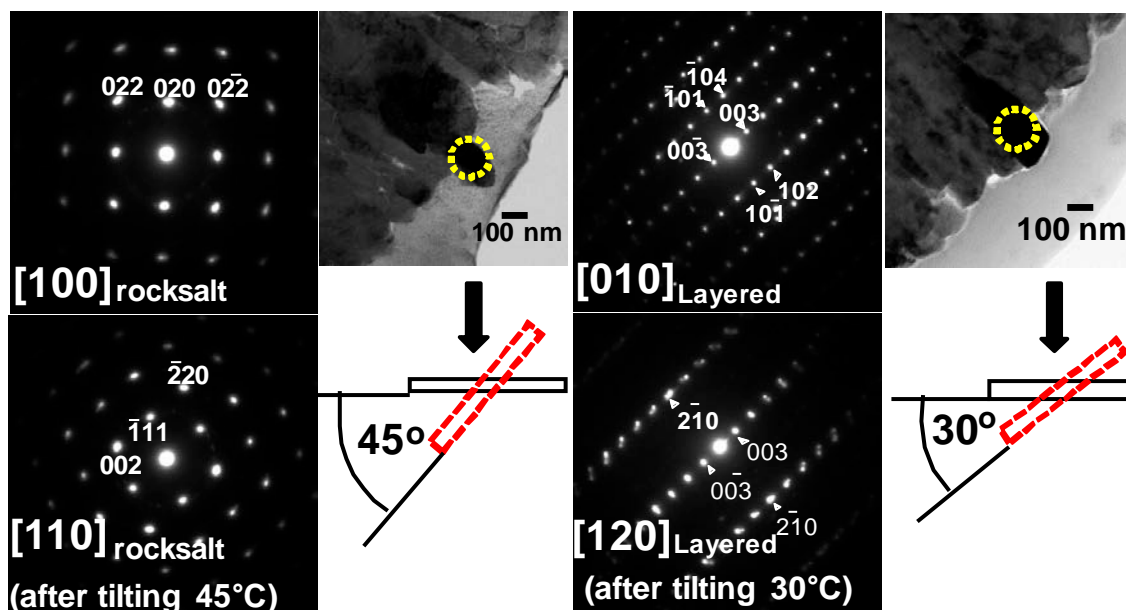


Fig. S2 SAED patterns from $Fm\bar{3}m$ and $R\bar{3}m$ primary particles in 1 mol% W-LNO. The SAED patterns were obtained from two different zones by tilting the sample as shown to ensure the phase identity.

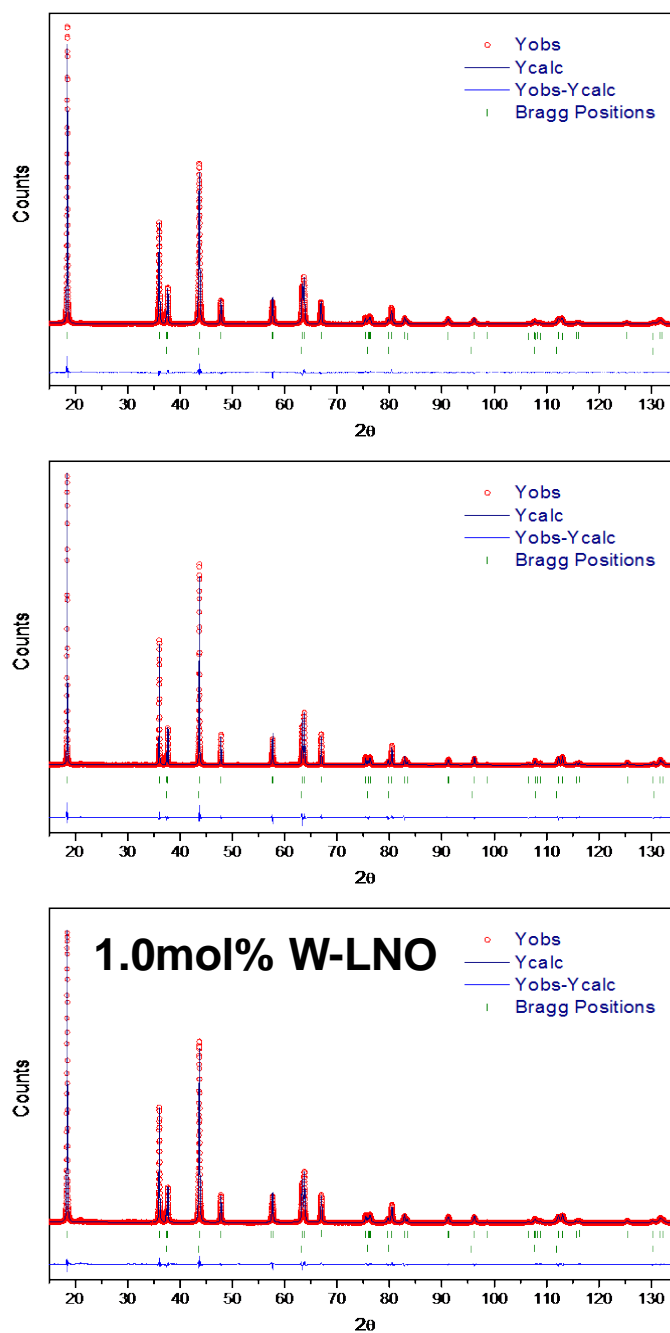


Fig. S3 XRD patterns and Rietveld refinement of as-prepared LNO, 0.5 mol% and 1 mol% W-LNO cathodes. Rietveld refinement produced the best fit as a mixture of $Fm\bar{3}m$ ($\text{Li}_{1/3}\text{Ni}_{2/3}\text{O}$) and $R\bar{3}m$ phases.

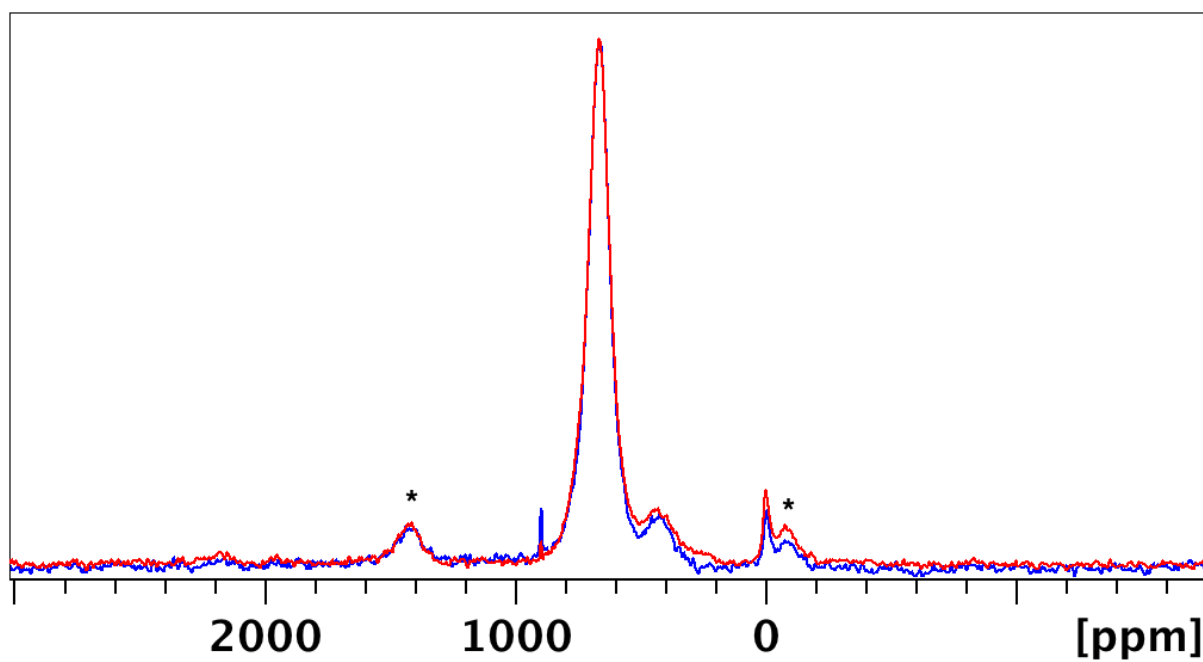


Fig. S4 ${}^6\text{Li}$ MAS NMR spectra of the pure, uncycled powder (blue) and the 1 mol% W-doped uncycled powder (red). Samples collected at 22 kHz spinning speed, at a resonance frequency of 29.48 MHz (4.7 T magnet). * indicate spinning sidebands.

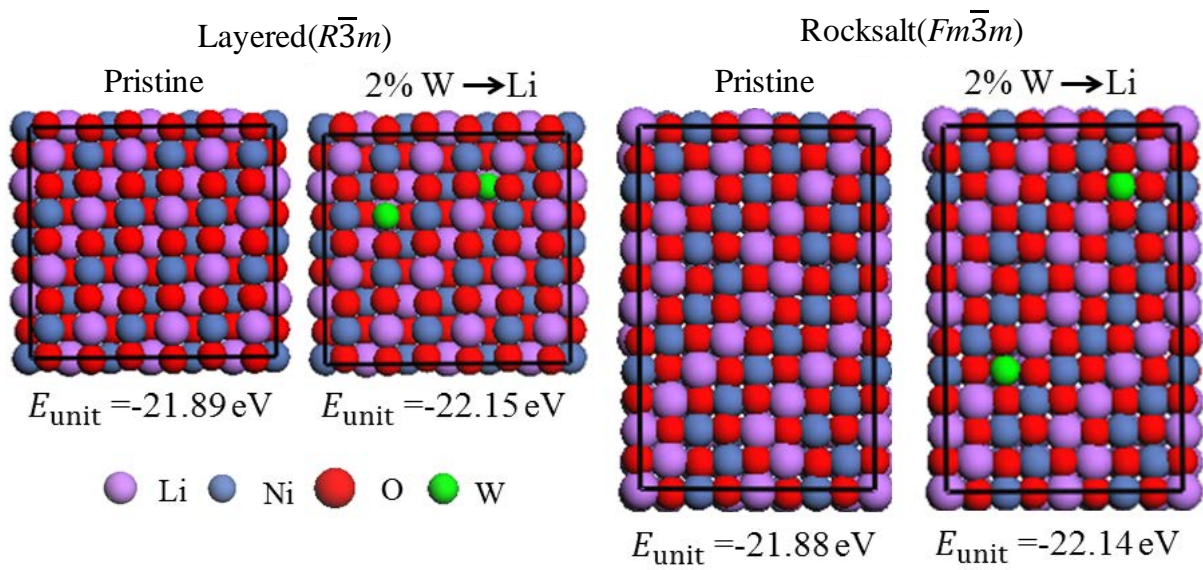


Fig. S5 Atomic structures of bulk hexagonal layered and rocksalt LNO without and with 2% W dopant. The total energies per unit formula are also listed.

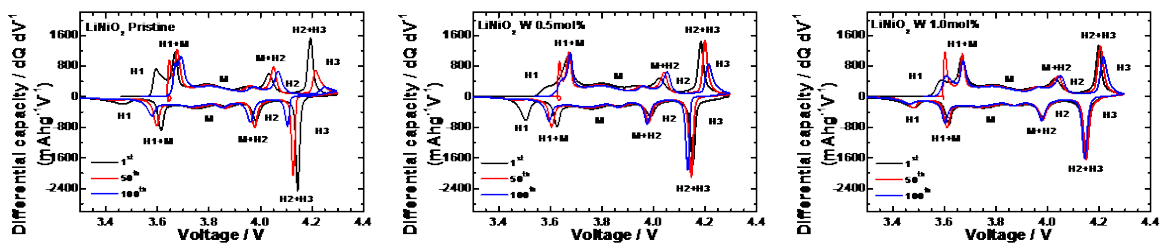


Fig. S6 $dQ dV^{-1}$ vs. V curves for the LNO, 0.5 mol%, and 1 mol% W-doped LNO cathodes at 1st, 50th, 75th, and 100th cycles. All cells were tested within voltage range of 2.7 – 4.3 V at 0.1 C and 30 °C in a half cell using Li metal anode. Phase transition during charging and discharging are labelled (H = hexagonal and M = monoclinic).

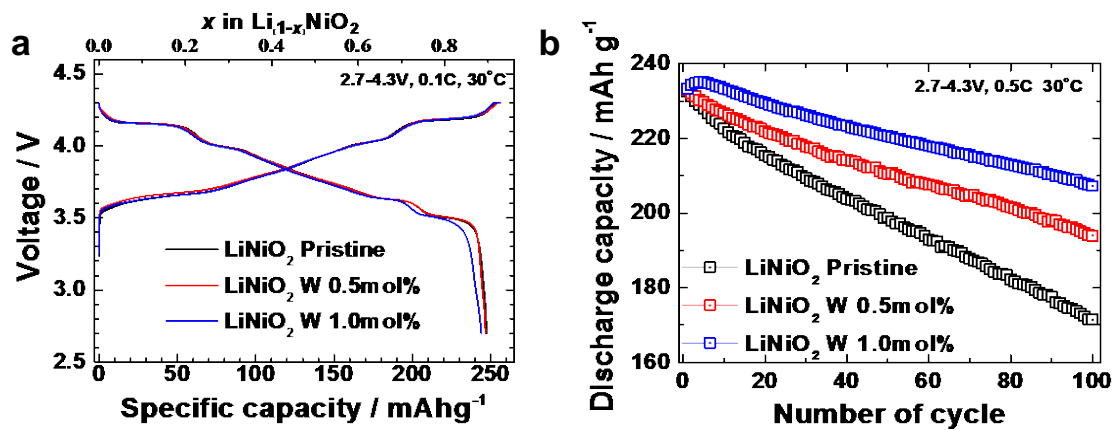


Fig. S7 (a) 1st cycle voltage profiles for pristine, 0.5 mol% and 1 mol% W-doped cathodes. All cells were operated within voltage range of 2.7 – 4.3 V at 0.1 C and 30 °C in a half cell using Li metal anode. (b) cycling performance of the cathodes in (a) tested at 0.5C.

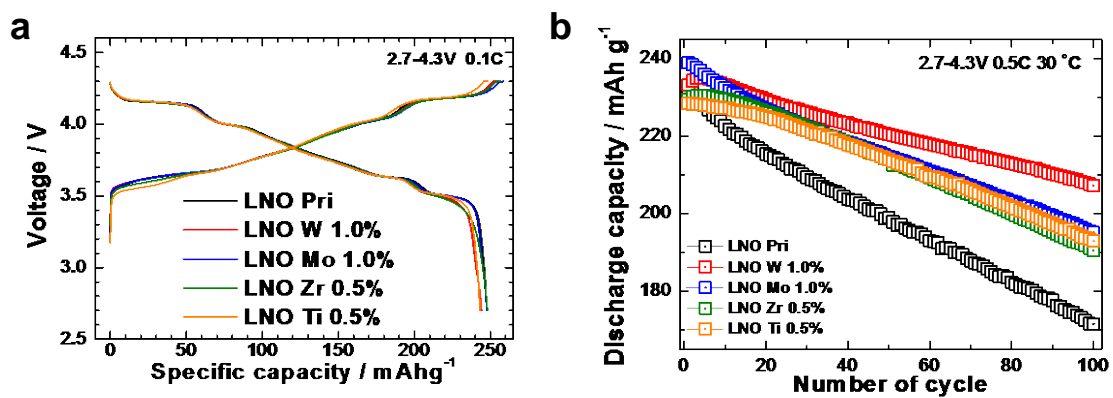


Fig. S8 (a) 1st cycle voltage profiles for the different dopants (Zr, Mo, Ti) and W-doped LNO performed cathodes. All cells were operated within voltage range of 2.7 – 4.3 V at 0.1 C and 30 °C in a half cell using Li metal anode. (b) cycling performance of the cathodes in (a) tested at 0.5C.

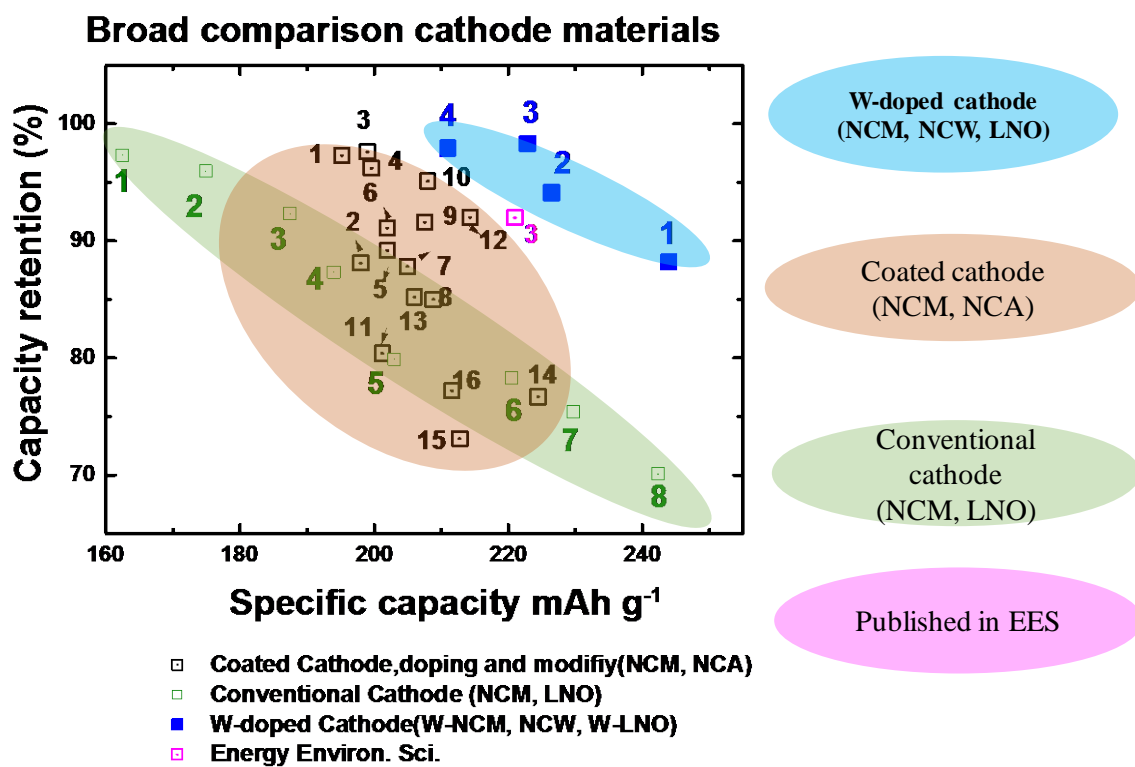


Fig. S9 Broad comparison of Ni-rich layered cathodes. The figure illustrates that the proposed W-doped Ni-rich layered cathodes clearly outperformed other Ni-rich layered cathodes with surface protections reported in the literature.

Table S1 Summary of Rietveld refinement of XRD patterns.^a Lattice parameter for the $Fm\bar{3}m$ phase

Composition	a (Å)	c (Å)	Weight fraction of rocksalt phase (%)	Li-O bond distance (Å)	Ni-O bond distance(Å)
LNO	2.87735(2)	14.1987(2)	2.8	2.1214(4)	1.9636(4)
	4.1015(8) ^a				
0.5 mol% W-LNO	2.87597(2)	14.2069(2)	4.4	2.1206(6)	1.9638(5)
	4.0962(8) ^a				
1 mol% W-LNO	2.87561(4)	14.2107(4)	4.8	2.1205(4)	1.9639(5)
	4.0980(7) ^a				

Table S2 The local and absolute average magnetic moments of Ni-ions in the different systems studied. The presence of Ni²⁺-type charge state is a result of W-doping. Spin flipping of Ni-ions is noted. The increase in average magnetic moment due to W-doping indicates charge compensation.

Local magnetic moments on Ni atoms (μB) ^a				
Li _{0.5} NiO ₂ (12 f.u.)	Li _{0.5} Ni _{0.916} W _{0.083} O ₂ (12 f.u.)	Li _{0.5} Ni _{0.937} W _{0.063} O ₂ (16 f.u.)	Li _{0.33} Ni _{0.67} O (8 f.u.)	Li _{0.33} Ni _{0.625} W _{0.0417} O (16 f.u.)
0.345	0.308	0.714	-1.192^b	1.054
0.663	0.729	1.256	1.15	-1.175^b
0.073	0.085	0.487	1.15	1.448
0.33	0.35	0.163	0.467	1.405
0.33	0.35	0.073	-1.192^b	1.467
0.073	0.085	0.077	0.468	1.366
0.663	0.729	0.107	1.143	-0.679 ^b
0.345	0.308	0.132	1.143	1.293
0.057	1.179	1.298		-1.149^b
0.623	0.605	0.21		0.591
0.133	1.176	0.24		-0.485 ^b
0.615		0.412		1.311
		0.34		1.424
		0.918		1.417
		0.824		1.323
Average absolute magnetic moments on Ni atoms (μB)				
Li _{0.5} NiO ₂ (12 f.u.)	Li _{0.5} Ni _{0.916} W _{0.083} O ₂ (12 f.u.)	Li _{0.5} Ni _{0.937} W _{0.063} O ₂ (16 f.u.)	Li _{0.33} Ni _{0.67} O (8 f.u.)	Li _{0.33} Ni _{0.625} W _{0.0417} O (16 f.u.)
0.35	0.53	0.48	0.98	1.17

^a Ni-ions with magnetic moments marked in bold are Ni²⁺ type ions. ^b Ni ions with spin flipping.

Table S3 Broad comparison of Ni-rich layered cathodes (pristine, coating, doping, and modify cation). The table illustrates that the proposed W-doped Ni-rich layered cathodes clearly outperformed other Ni-rich layered cathodes with surface protections reported in the literature.

#Num	W-doped cathode Composition	Discharge Capacity (mAh g ⁻¹)	Current density (1C, mA g ⁻¹)	100 cycles Capacity retention (%), 0.5C	Mass loading of AM (mg cm ⁻²)	AM: Conductor: Binder	Our Results (This work)
1	W-LNO	244	180 2.7-4.3V	88.2	4.5	90: 5.5: 4.5	
2	W-NCM 900505	226.5		94.1			
3	W-NC 8911	222.9		98.3			
4	W-NCM 801505	211		97.9			

Num.	Conventional cathode Composition	Discharge Capacity (mAh g ⁻¹)	Current density (1C, mA g ⁻¹) 2.7-4.3V	100 cycles Capacity retention (%), 0.5C	Mass loading of AM (mg cm ⁻²)	AM: Conductor: Binder	Reference
1	NCM 333	162.5	200	97.3	-	85: 7.5: 7.5	5
2	NCM 523	174.9		95.9			
3	NCM 622	187.4		92.3			
4	NCM 701515	194.0		87.3			
5	NCM 811	203.0		79.9			
6	NCM 90 05 05	220.5	200	78.3	-	85: 7.5: 7.5	6
7	NCM 95 2.5 2.5	229.7		75.4			
8	LNO	242.4		70.1			

Num.	Coated cathode Composition	Coating/doping Source & modification	Method	Current density (1C, mA g ⁻¹)	0.1C Discharge Capacity (mAh g ⁻¹)	100 cycles Capacity retention (%)	Mass loading of AM (mg cm ⁻²)	AM: Conductor: Binder	Reference
------	----------------------------	--------------------------------------	--------	---	--	-----------------------------------	---	-----------------------	-----------

					Before treated	After treated			
1	NCM 333	LiTaO ₃	ALD	160	145(3.0-4.5V)	93	-	80: 10: 10	7
2	LFP	Lithium-excess		160	140 2.95C	500/ 81.5 % 100/ 96.5 %	~ 3.1	70: 20: 10	8
3	NCM 850510	TSFCG	-	200	221 (2.7~4.3V)	92	1.3	85: 7.5: 7.5	9

Num.	Coated cathode Composition	Coating/doping Source & modification	Method	Current density (1C, mA g ⁻¹)	0.1C Discharge Capacity (mAh g ⁻¹)		Normalized 100 cycles Capacity retention (%)	Mass loading of AM (mg cm ⁻²)	AM: Conductor: Binder	Reference
					Before treated	After treated				
1	NCM 811	Li ₂ ZrO ₃	Wet coating	180 (2.8~4.3V)	195.2	97.3(1C)	-	80: 10 :10	10	
2		Li ₃ PO ₄ , Polypyrrol e	Wet coating & polymerization	200 (2.0~4.5V)	198	88.1(1C)	-	80: 10: 10	11	
3		SO ₄ ²⁻ /ZrO ₂	Wet coating	200 (3.0~4.3V)	199	97.6(1C)	9.5	92: 4: 4	12	
4	NCA 80 15 05	LiMnPO ₄		(2.8~4.3V)	199.6	96.2(1C)	-	75: 20: 5	13	
5	NCM 811	V ₂ O ₅		200 (2.8~4.3V)	202	89.2(2C)	-	80: 10 :10	14	
6		LiF		(2.8~4.3V)	202	91.1(2C)	-	80: 10 :10	15	
7		AlF ₃	200 (3.0~4.3V)	205	87.8(0.5C)	-	85: 7.5 :7.5	16		
8	NCM 88 10 02	Na ₂ SO ₄	190 150	206	85.2(1C)	10	76.9: 7.7 :15.4	17		

				(2.8~4.3V)					
9	NCA 80 15 05	Co ₃ O ₄		(2.8~4.3V)	207.6	91.6(1C)	-	80: 10 :10	18
10	NCM 811	SiO ₂		(2.8~4.3V)	208	95.1(1C)	-	80: 10 : 0	19
11	NCM 811	silkworm-like structure	-	200 (2.7~4.3V)	201.2	80.4 (1C)	2.6	80: 10 :10	20
12	NCM 80 15 05	Residual Li remove	wet coating (solvent evaporation)	175 (2.5~4.3V)	214.3	92(1C)	10	92: 4 :4	21
13	NCM 85 15 05	Co/P-coated 1:1	Wet coating	175	208.8	85(1C)	10	92: 4 :4	22
14	NCM 91 06 03	Co ₃ (PO ₄) ₂	Dry coating		224.5	76.7(1C)	10	92: 4 :4	23
15		Mn ₃ (PO ₄) ₂			212.8	73.1(1C)			
16		Fe ₃ (PO ₄) ₂			211.6	77.2(1C)			

Notes and references

- 1 G. Kresse, and J. Furthmüller, *Phys. Rev. B*, 1996, **54**, 11169.
- 2 Y. Chen, F. Peng, Y. Yan, Z. Wang, C. Sun, and Y. Ma, *J. Phys. Chem. C*, 2013, **117**, 13879.
- 3 J. P. Perdew, K. Burke, and M. Ernzerhof, *Phys. Rev. Lett.*, 1996, **77**, 3865.
- 4 S. L. Dudarev, G. A. Botton, S. Y. Savrasov, C. J. Humphreys, and A. P. Sutton, *Phys. Rev. B*, 1998, **57**, 1505.
- 5 H.-J. Noh, S. Yoon, C. S. Yoon, and Y.-K. Sun, *J. Power Sources*, 2013, **233**, 121.
- 6 Chong S. Yoon, M. H. Choi, B.-B. Lim, E.-J. Lee, and Y.-K. Sun, *J. Electrochem. Soc.*, 2015, **162** A2483.
- 7 X. Li, J. Liu, M. Norouzi Banis, Lushington, R. Li, M. Cai, and X. Sun, *Energy Environ. Sci.*, 2014, **7**, 768.
- 8 K.-Y. Park, I. Park, H. Kim, G. Yoon, H. Gwon, Y. Cho, Y. S. Yun, J.-J. Kim, S. Lee, D. Ahn, Y. Kim, H. Kim, I. H., W.-S. Yoon, and K. Kang, *Energy Environ. Sci.*, 2016, **9**, 2902.
- 9 J. H. Lee, C. S. Yoon, J.-Y. Hwang, S.-J. Kim, F. Maglia, P. Lamp, S.-T. Myung, and Y.-K. Sun, *Energy Environ. Sci.*, 2016, **9**, 2152.
- 10 H. Liang, Z. Wang, H. Guo, J. Wang, and J. Leng, *Applied Surface Science*, 2017, **423**, 1045.
- 11 S. Chen, T. He, Y. Su, Y. Lu, L. Bao, L. Chen, Q. Zhang, J. Wang, R. Chen, and F. Wu, *ACS Appl. Mater. Interfaces*, 2017, **9**, 29732.
- 12 S.-G. Woo, J. H. Han, K. J. Kim, J.-H. Kim, J.-S. Yu, and Y.-J. Kim, *Electrochimica Acta*, 2015, **153**, 115.
- 13 J. Duan, C. Wu, Y. Cao, K. Du, Z. Peng, and G. Hu, *Electrochimica Acta*, 2016, **221**, 14.
- 14 X. Xiong, Z. Wang, G. Yan, H. Guo, and X. Li, *J. Power Sources*, 2014, **245**, 183.
- 15 X. Xiong, Z. Wang, X. Yin, H. Guo, and X. Li, *Materials Letters*, 2013, **110**, 4.
- 16 S.-U. Woo, C. S. Yoon, K. Amine, I. Belharouak, and Y.-K. Sun, *J. Electrochem. Soc.*, 2007, **154**, 1005.
- 17 J. W. Choi, J. W. Kim, K.-T. Lee, J. H. Lim, J. H. Lee, and Y. S. Yun, *Adv. Mater. Interfaces*, 2016, **3**, 1600784.
- 18 Y. Huang, Y. Huang, and X. Hu, *Electrochimica Acta*, 2017, **231**, 294.
- 19 L. Liang, G. Hu, F. Jiang and Y. Cao, *J. Alloys, and Compounds*, 2016, **657**, 570.
- 20 C. Zhanga, J. Qi, H. Zhao, H. Hou, B. Deng, S. Tao, X. Su, Z. Wang, B. Qian, and W. Chu, *Materials Letters*, 2017, **201**, 1.
- 21 K. J. Park, J.-H. Park, S.-G. Hong, B. J. Choi, S. Heo, S.-W. Seo, K. M. Min, and J. H. Park, *Sci. Rep*, 2017, **7**, 44557.
- 22 K. J. Park, J.-H. Park, B. J. Choi, J. H. Kim, S. G. Hong, and H. N. Han, *Electrochimica Acta*, 2017, **257**, 217.
- 23 K. M. Min, K. J. Park, S. Y. Park, S.-W. Seo, B. J. Choi, and E. S. Cho, *Sci. Rep*, 2017, **7**, 7175.